SEAMLINE OPTIMIZATION FOR UAV IMAGE MOSAICKING USING GEOMETRY OF TRIANGULATED IRREGULAR NETWORK

S. Yoon [1] and T. Kim [1]*

[1] Dept. of Geoinformatic Engineering, Inha University, Incheon, S. Korea - 22181415@inha.edu, tezid@inha.ac.kr

KEY WORDS: Image Mosaicking, Triangulated Irregular Network, UAV Block Adjustment, Relief Displacement, Error-prone Region.

ABSTRACT:

For efficient UAV (Unmanned Aerial Vehicle) image monitoring, it is essential to mosaic multiple UAV images into one seamless image. In a mosaicked image, relief displacement of terrain is a major source of error. It is difficult to form seamlines that avoid all areas of relief displacements. A seamline determination method alone is limited in reducing the mismatch error on mosaicked image. In this study, we constructed a TIN (Triangulated Irregular Network) using tiepoints generated by rigorous bundle adjustments. We detected the regions where relief displacement occurred using the slope of TIN facets. It was found that the error of mosaicked image were mostly on TIN facets with high slopes. Our method generated a mosaicked image after elimination of error-prone region and showed that the distortions were effectively removed. This study showed that the proposed method could produce mosaicked images with stable quality using geometric clues of TIN. We expected that our method can be used for UAV image mosaicking robust to mismatching factors.

1. INTRODUCTION

UAV (Unmanned Aerial Vehicle) image mosaicking uses multiple UAV images to produce one seamless image. In this process, relief displacement of terrain is a major source of error. Typical mosaicking techniques assign pixel values to a mosaicked image according to a continuous terrain model such as DSM (Digital Surface Model) (Zhang et al., 2023). As a result, errors due to relief displacement appear in the form of distortion in the mosaicked image. It is also very difficult to prepare a perfect DSM without such displacement errors.

In contrast, mosaicking techniques that do not utilized DSMs stitch images to a reference plane only using EOPs (Exterior Orientation Parameters) of images. Errors appear in the form of mismatches at the seamlines between images. In this case, it is important to determine the optimal seamlines minimizing relief displacement. Related research has mainly focused on the pattern of brightness in UAV images. The application such as optical flow (Zhang et al., 2018) and super-pixel (Yuan et al., 2020a) algorithms were tried. In addition, there have been studies that apply deep learning to pixel values for optimization of seamline (Li et al., 2017; Yuan et al., 2020b). However, seamlines passed through relief displacement regions such as building rooftops, and severe mismatches occurred. The related studies indicated that it was difficult to form a seamlines that avoids all areas of relief displacements, and that the seamline determination method using only pixel values was limited in reducing the mismatch error on mosaicked image.

In this study, we constructed a TIN (Triangulated Irregular Network) using tiepoints generated by rigorous bundle adjustments (Yoon and Kim, 2022). We detected the regions where relief displacement occurred using the slope of TIN facets. We removed them to determine optimal seamlines for image mosaicking.

2. MATERIALS AND METHODS

KD-2 Mapper SmartOne

Figure 1. Appearances of the UAV used

Specification		Dataset 1	Dataset 2
UAV	Name	KD-2 Mapper	SmartOne
	Manufacturer	Keva Drone	Smartplanes
	Flight type	fixed wing	fixed wing
	Positioning sensor	DGPS	DGPS
Image size		7952 × 3264	4928 × 3264
Number of images		60	58
Overlap (%)	Endlap	70	70
	Sidelap	80	80
Height of flight (m)		180	150
GSD (m)		0.0242	0.0389

Table 1. Descriptions of the dataset information

* Corresponding author

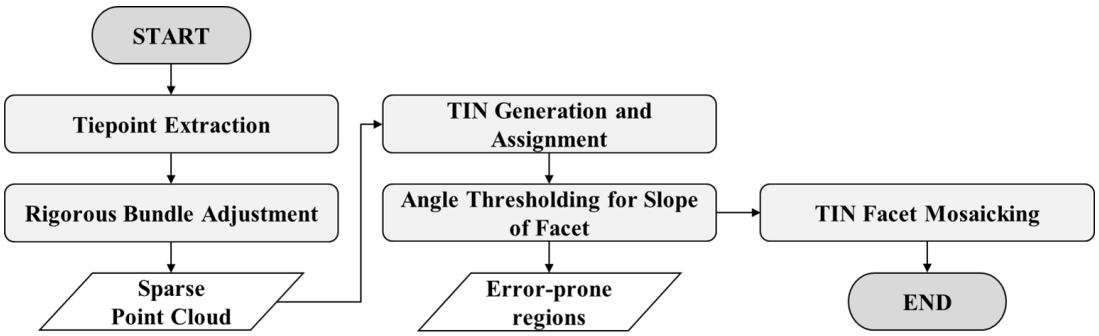

Figure 2. Flowchart of the proposed method

For our experiments, we used two datasets described in Table 1. Dataset 1 was acquired with the KD-2 Mapper UAV shown in Figure 1. The UAV is fixed-wing and applies a DGPS (Differential Global Positioning System) to obtain position information with typical accuracy. Dataset 1 is dominated by a plane with a few buildings. In this area, the UAV flew at a height of 180 meters, and the GSD (Ground Sample Distance) of the image was 2.4 centimeters. The number of images acquired is 60. Dataset 2 was acquired with a SmartOne UAV. Similar to the KD-2 Mapper UAV, this UAV is fixed-wing and uses DGPS for positioning. Dataset 2 is also dominated by plane with a few buildings. In this area, the UAV flew at a height of 150 meters, and the GSD of the image was 3.9 centimeters. The number of acquired images is 58. Using these two datasets, we tried to compare the results of the mosaic in the plane and building areas. The mosaic results in the plane area can show the overall performance of the proposed algorithm. Furthermore, the mosaic results in the building area can describe the extent to which the error is reduced by the proposed algorithm.

Figure 2 shows the flowchart of the proposed method. First, tiepoints are generated for bundle adjustment. Tiepoints are determined between each pair-images and extracted by the SURF (Speeded Up Robust Features) algorithm. Then, the EOPs of the images are corrected and the model coordinates of each tiepoint are calculated through block adjustment. Next, a TIN is constructed using these tiepoints. These TINs are assigned to the coverage of each image, and the slopes of each facet are calculated. By thresholding the slopes, the facets with the higher slopes are extracted, and these are selected as the final error-prone regions. Image mosaicking is then performed using the inlier facets. The details are described in the following subsections.

2.1 Rigorous Bundle Adjustment

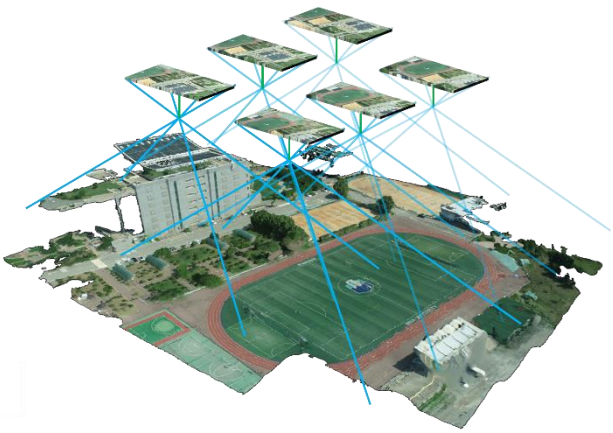

Figure 3. UAV photogrammetric block adjustment

Block adjustment is a technique that simultaneously corrects the EOPs of all acquired UAV images and the ground coordinates of the tie points, as shown in Figure 3. Therefore, the quality of the tie points is important. Before the block adjustment is performed, the outliers in the tie points are first removed using the RANSAC (Random Sample Consensus) algorithm. A coplanarity model was applied to RANSAC, and its operation was repeated until the model accuracy was within 3 pixels. The three-dimensional ground coordinates of the tie points were then estimated along the coplanarity model. By re-projecting these ground coordinates onto another image, the distance difference between the original and projected image coordinates was determined as shown in Figure 4. The projection from ground coordinates to image coordinates is calculated according to the collinearity model as Equation (1). In this study, tie points with a reprojection error of more than 3 pixels were removed.

$$x_n = -f\frac{r_{11}(X_n - T_x) + r_{12}(Y_n - T_y) + r_{13}(Z_n - T_z)}{r_{31}(X_n - T_x) + r_{32}(Y_n - T_y) + r_{33}(Z_n - T_z)}$$
$$y_n = -f\frac{r_{21}(X_n - T_x) + r_{22}(Y_n - T_y) + r_{23}(Z_n - T_z)}{r_{31}(X_n - T_x) + r_{32}(Y_n - T_y) + r_{33}(Z_n - T_z)} \quad (1)$$

where X_n, Y_n, Z_n = nth object coordinates in the model coordinate system
x_n , y_n = nth object coordinates in the image coordinate system
$r_{11\ to\ 33}$ = rotation elements for EOP
T_x, T_y, T_z= translation elements for EOP
f = focal length
n = 1 to the number of features

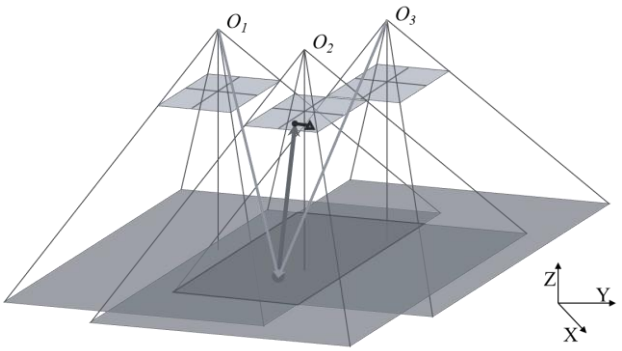

Figure 4. reprojection error verification on our study

The collinearity condition as in equation (1) was adopted as the block adjustment model in this study. The block adjustment was applied to recursive LSE (Least Square Estimation), where weights and constraints were used. This was constructed as shown in Equation (2). In this experiment, the initial weights were set as shown in Table 2, considering the measurement error range. Then, as the iterative block adjustment proceeded, the covariance matrix was calculated from the residuals. Based on covariance matrix calculated, the weights were automatically updated.

$$W\bar{B}\Delta = W\bar{C} + \bar{V}$$

$$\begin{pmatrix} W & 0 & 0 \\ 0 & \dot{W} & 0 \\ 0 & 0 & \ddot{W} \end{pmatrix} \begin{pmatrix} \dot{B} & \ddot{B} \\ I & 0 \\ 0 & I \end{pmatrix} \begin{pmatrix} \dot{\Delta} \\ \ddot{\Delta} \end{pmatrix} = \begin{pmatrix} W & 0 & 0 \\ 0 & \dot{W} & 0 \\ 0 & 0 & \ddot{W} \end{pmatrix} \begin{pmatrix} \epsilon \\ \dot{C} \\ \ddot{C} \end{pmatrix} + \begin{pmatrix} v \\ \dot{V} \\ \ddot{V} \end{pmatrix} \quad (2)$$

where W, $\dot{W}$, $\ddot{W}$ = weights of increments for EOP and ground coordinates of tie points
$\dot{B}$, $\ddot{B}$ = coefficients of partial differential equations for EOP and ground coordinates of tie points in collinearity conditions
I = coefficients of identity matrix
$\dot{\Delta}$, $\ddot{\Delta}$ = increments for EOP and ground coordinates of tie points
ϵ = differences between observed and initial values for collinearity equations
$\dot{C}$, $\ddot{C}$ = differences between observed and initial values for EOP and ground coordinates of tie points
v = residuals for collinearity equations
$\dot{V}$, $\ddot{V}$ = residuals for EOP, ground coordinates of tie points

Parameters	Initial weight
Model (pixel)	1.0
EOP's rotation (degree)	10.0
EOP's translation (m)	1.0

Table 2. Initial weights for block adjustment

2.2 TIN Generation and Assignment

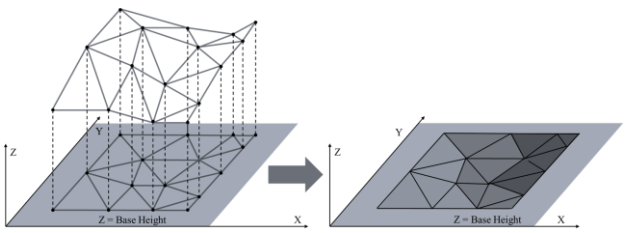

Figure 5. Concept of TIN generation and assignment

After bundle adjustment, tiepoints have corrected ground coordinates. In this paper, these points are defined as rapid point cloud. This rapid point cloud can describe the terrain of the target area. Therefore, it is the key to the mosaic generation in the proposed method. In most cases, the number of tiepoints within this point cloud is excessive. They need to be sampled to reduce the computational complexity. In this study, the rapid point cloud was sampled at 5 meters intervals in the model space.

A TIN in the model space is formed by the rapid point clouds, as shown in Figure 5. It is based on the Delaunay triangulation algorithm, which is available in the OpenCV library. The TINs are then projected onto a reference plane to generate a mosaicked image, and the range of the TINs is formed as the range of the mosaicked image.

2.3 TIN Facet Mosaicking

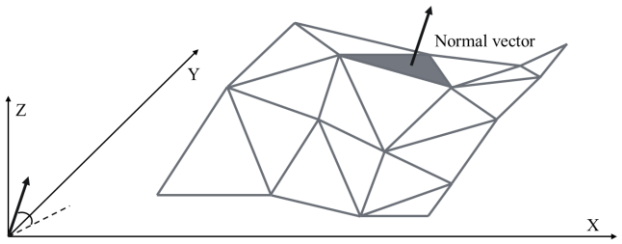

Figure 6. Concept of TIN facet's slope

As shown in the introduction section, relief displacement is a major source of error in mosaicked images. This study aims to detect these errors based on the slopes of each TIN's facet. These slopes are calculated as shown in Equations (3) and (4).

$$\vec{n} = \begin{bmatrix} n_1 \\ n_2 \\ n_3 \end{bmatrix} = \overrightarrow{P_1P_2} \times \overrightarrow{P_1P_3} \quad (3)$$

$$\theta = \frac{\pi}{2} - \cos^{-1}\left(\frac{n_1^2 + n_2^2}{\sqrt{n_1^2 + n_2^2 + n_3^2}\sqrt{n_1^2 + n_2^2}}\right) \quad (4)$$

where n_1, n_2, n_3 = components of normal vector
P_1, P_2, P_3 = three random points in a vector space
θ = slope of a plane with three points P_1, P_2, P_3

The slope becomes larger in areas where there are tall objects such as buildings. Relief displacements are also likely to occur. Therefore, facets with slopes above a certain angle could be defined as error-prone regions. In this study, we checked the error-prone region extraction results for three different slopes: 30, 40, and 60 degrees.

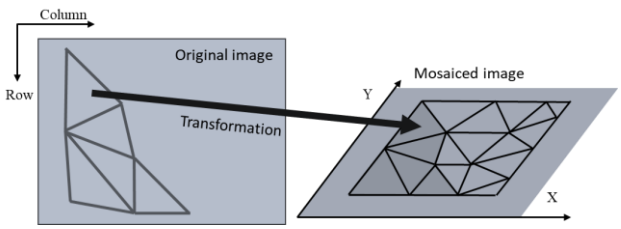

Figure 7. Concept of mosaicking using TIN facet

The TIN facets assigned to the image are used as the units of the image mosaic. The transformation relationship from the original image to the mosaicked image is estimated by the affine transformation model for the corner points of the facet. The affine transformation model can represent the translation, rotation, and scaling of the image, and can be estimated with only three points. The affine transformation model is shown in Equation (5).

$$\begin{bmatrix} x' \\ y' \\ 1 \end{bmatrix} = \begin{bmatrix} r_1 & r_2 & t_1 \\ r_3 & r_4 & t_2 \\ 0 & 0 & 1 \end{bmatrix} \begin{bmatrix} x \\ y \\ 1 \end{bmatrix} \quad (5)$$

where x, y = image coordinate of an original point
x', y' = image coordinate of a transformed point
r_i = rotation coefficients on affine model
t_j = translation coefficients on affine model

After the transformation relationship is estimated, the image facets are stitched into the mosaic image through image warping. The process is repeated for all the facets of the TIN, generating a mosaic image. Finally, the entire image patches are stitched to the error-prone regions on mosaic image.

3. RESULTS AND DISCUSSION

Tables 3 and 4 describe the block adjustment results for Datasets 1 and 2. For Dataset 1, 240794 tie points were extracted and used for block adjustment. In the estimation, the sigma not of the EOP was about 0.001. This meant that the estimated model was stable. After correcting the EOP, the model error was 1.2974 pixels, and the Y-parallax was 1.0165 pixels. From these accuracies, we could confirm that the relative error in the model space is small. For Dataset 2, 160949 tie points were used for block adjustment. Similar to Dataset 1, the sigma not of the EOP was found to be around 0.001. The model error was 1.2558 pixels, and the Y-parallax was 0.9263 pixels.

Dataset ID		1
Number of tiepoints		240794
Sigma not	Model	0.9360
	Rotation of EOPs	0.0011
	Translation of EOPs	0.0013
Model error (pixel)		1.2974
Y-parallax (pixel)		1.0165
Processing time (second)		301

Table 3. Results of block adjustment for dataset 1

Dataset ID		2
Number of tiepoints		160949
Sigma not	Model	0.3380
	Rotation of EOPs	0.0017
	Translation of EOPs	0.0015
Model error (pixel)		1.2558
Y-parallax (pixel)		0.9263
Processing time (second)		200

Table 4. Results of block adjustment for dataset 2

Tables 5 and 6 show the results for TIN facet mosaicking. For Dataset 1, 85181 rapid point clouds were extracted from 240794 tie points by re-projection error verification. Then, through sampling at 5 meters intervals, 6655 points were selected to be used for mosaicking. The TIN generated from this final rapid point cloud consisted of 13272 facets, as shown in Figure 8. For Dataset 2, 39984 rapid point clouds were extracted, and 4044 points were determined to be used for mosaicking. The generated TIN consisted of 7688 facets, as shown in Figure 9.

Dataset ID	1
Number of initial points on point cloud	85181
Number of sampled points on point cloud	6655
Number of TIN facets	13272
Processing time (second)	50

Table 5. Results of TIN facet mosaicking for dataset 1

Dataset ID	2
Number of initial points on point cloud	39984
Number of sampled points on point cloud	4044
Number of TIN facets	7688
Processing time (second)	39

Table 6. Results of TIN facet mosaicking for dataset 2

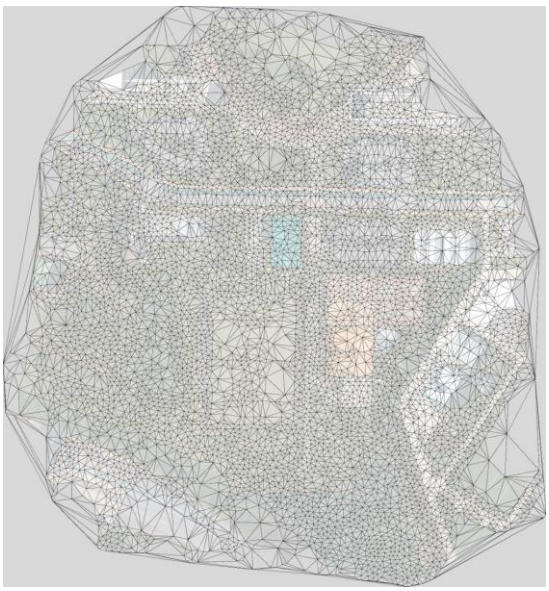

Figure 8. TIN generation result for dataset 1

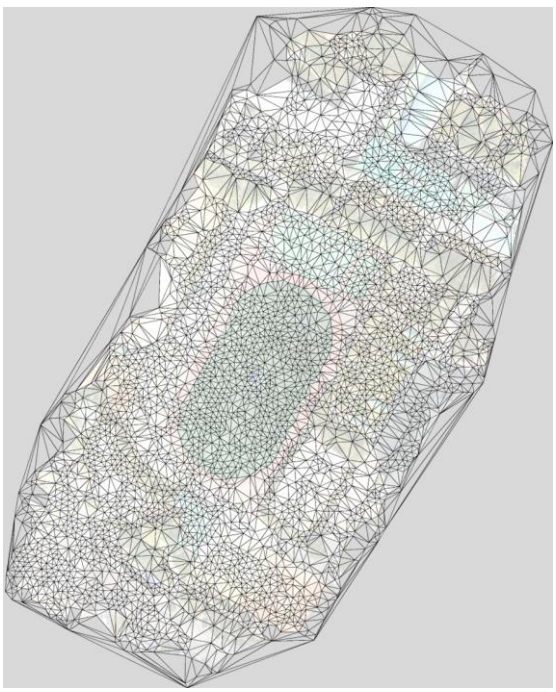

Figure 9. TIN generation result for dataset 2

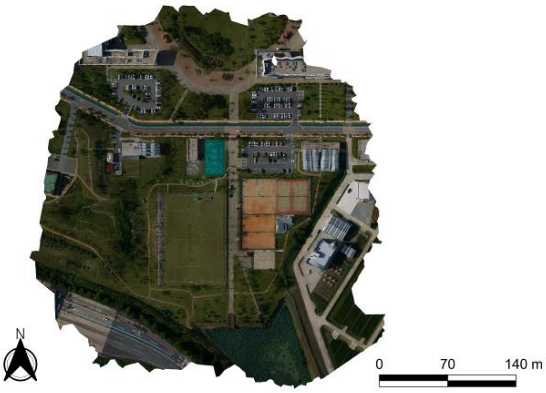

Figure 10. Initial mosaicked image for dataset 1

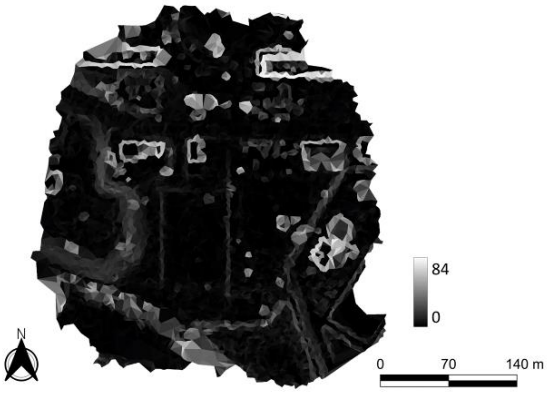

Figure 11. Slopes map for the TIN for dataset 1

Slope threshold is 30 degrees	Slope threshold is 45 degrees	Slope threshold is 60 degrees
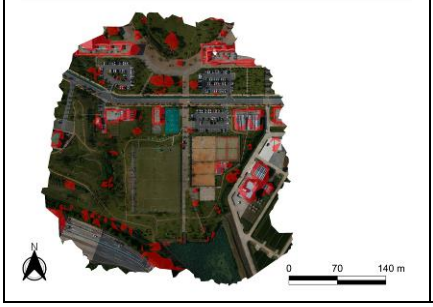	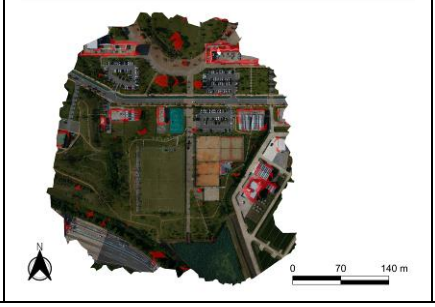	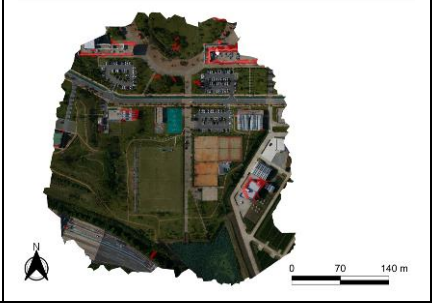

Figure 12. Relief displacement regions detected for each slope threshold from 30 to 60 degrees for dataset 1

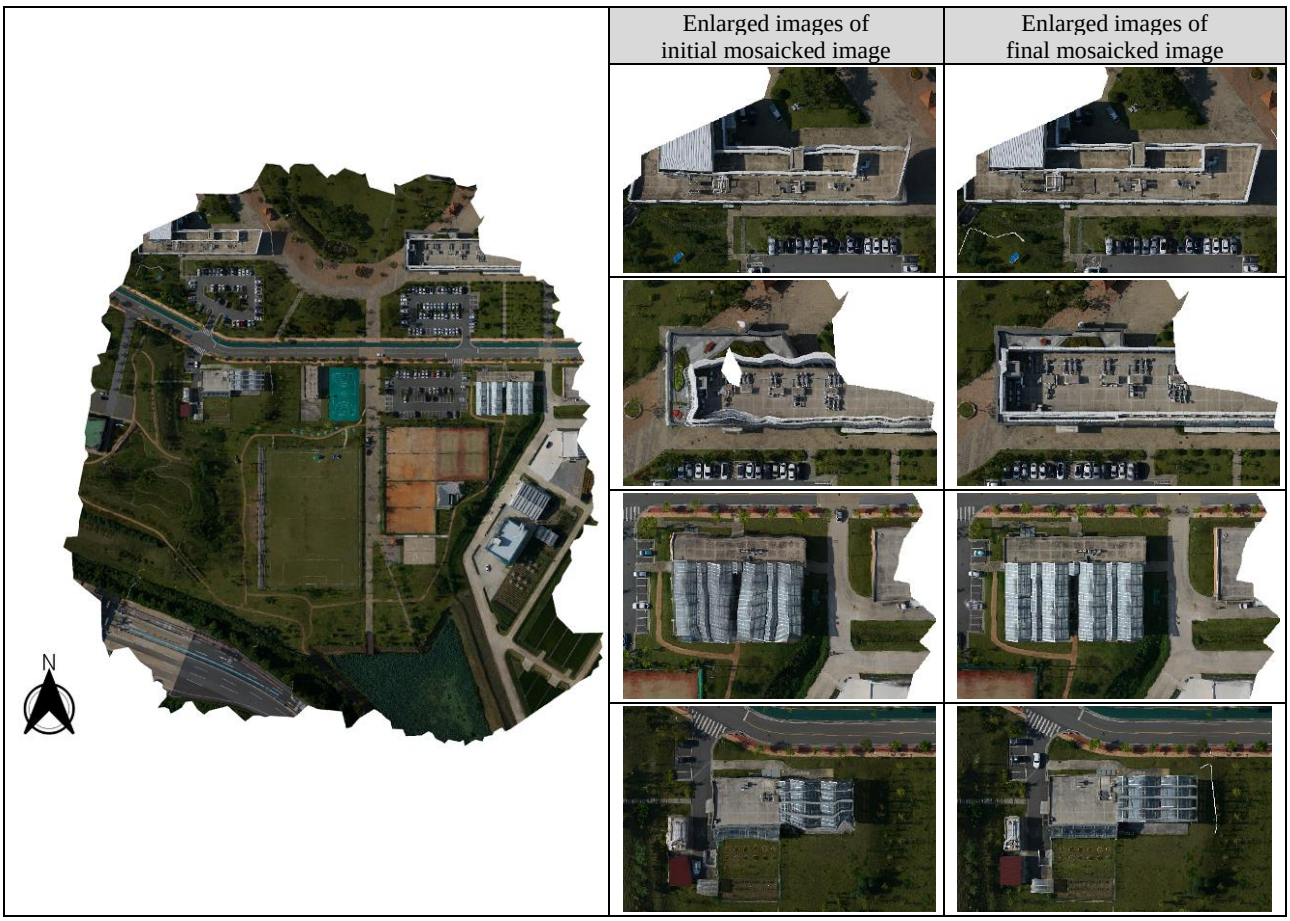

Figure 13. Final mosaicked image of proposed method for dataset 1

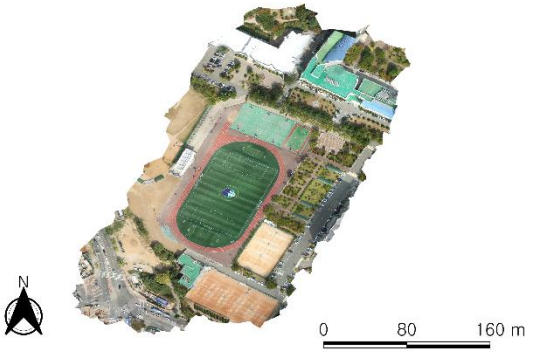

Figure 14. Initial mosaicked image for dataset 2

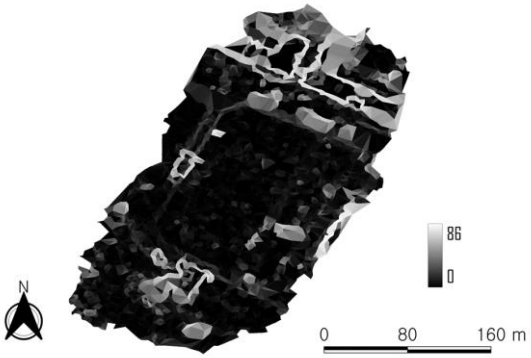

Figure 15. Slopes map for the TIN for dataset 2

Slope threshold is 30 degrees	Slope threshold is 45 degrees	Slope threshold is 60 degrees
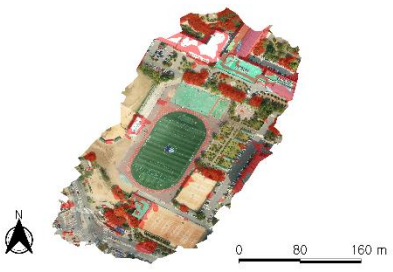	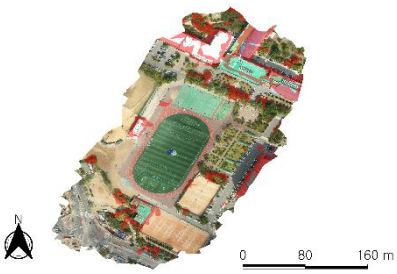	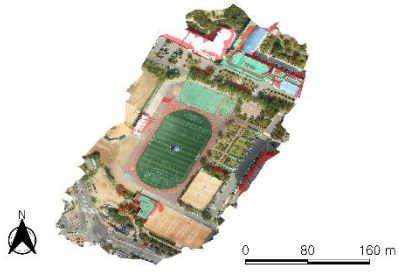

Figure 16. Relief displacement regions detected for each slope threshold from 30 to 60 degrees for dataset 2

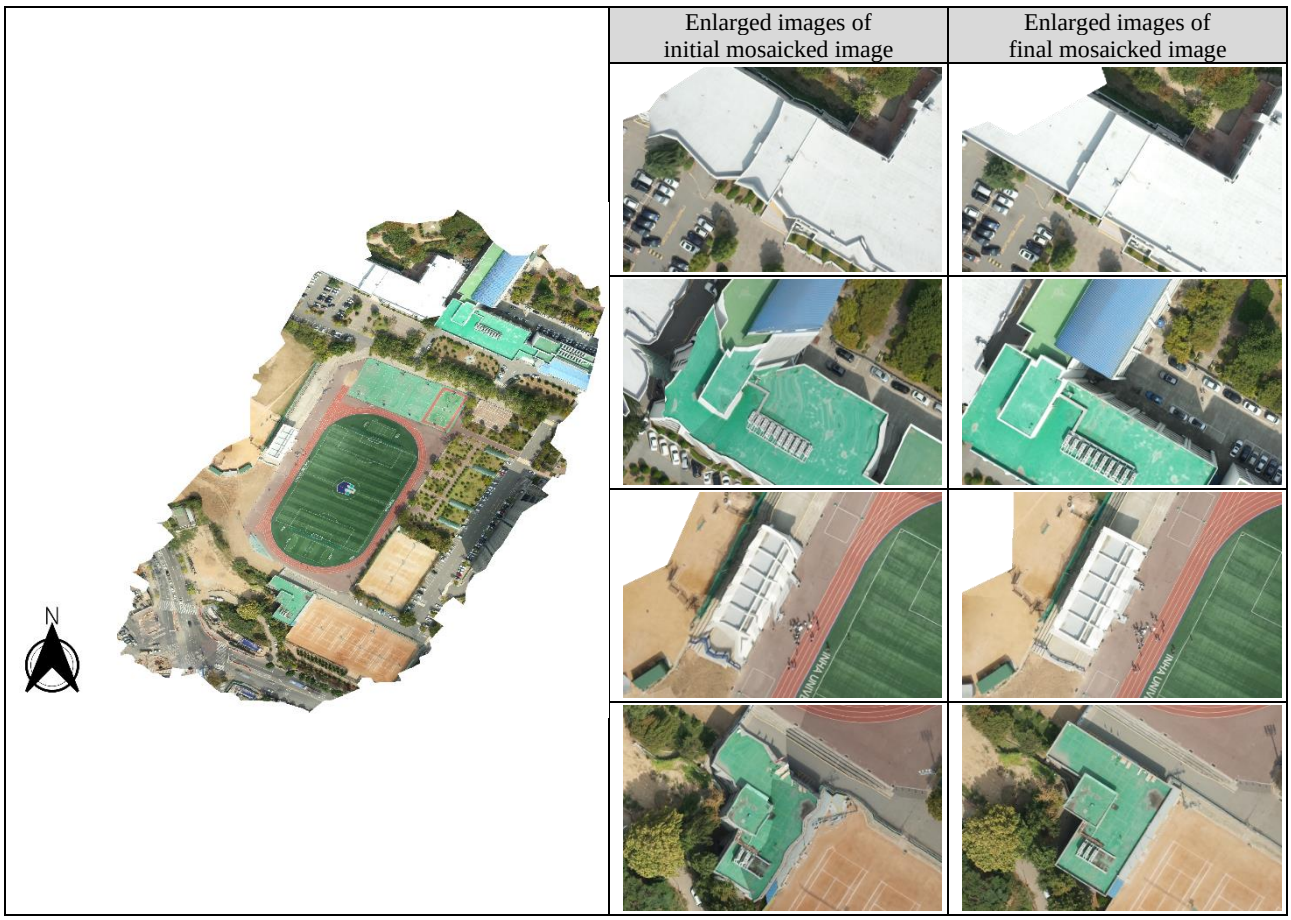

Figure 17. Final mosaicked image of proposed method for dataset 2

Figure 10 shows the initial mosaicked image and slope map for Dataset 1. The Facets with high slopes were located on trees, buildings, etc. The mosaic image was distorted within the region of those facets. The results for Dataset 2 in Figure 14 are similar to the results for Dataset 1. The results of thresholding for slopes are shown in Figures 12 and 16. As we increased the threshold value from 30 to 60, only facets around relatively high building areas were extracted. Therefore, by comparing the initial mosaic results with the error-prone regions extraction results, we determined the optimal slope threshold value. In this experiment, we determined 45 degrees as the optimal threshold value. Figures 13 and 17 show the final mosaic results after removing the error-prone regions. The error-prone regions in the initial mosaic image were successfully removed in the final mosaic image.

4. CONCLUSIONS

In this study, we utilized TINs for UAV image mosaicking. We aimed to verify a TIN can be utilized to mosaic UAV images without a DSM when the TIN was constructed from multiple image points generated through rigorous bundle adjustment. We also tried to reduce the mismatching error at the junction areas caused by relief displacements. An area with several buildings on a flat surface was selected as the target area, and the images were taken using a fixed-wing UAV.

We first generated a mosaicked image using the initial seamline constructed with a TIN. Errors caused by relief displacement appeared in the form of mismatches at the seamlines. When compared to the slope of TIN facets, severe distortions were mostly on facets with high slopes. The detected relief displacement regions for various slope thresholds showed that buildings at various sizes could be detected. Finally, the mosaicked image generated after elimination of error-prone region showed that seamlines and mismatches due to buildings were removed.

This study showed that the proposed method could produce mosaicked images with stable quality using geometric clues of a TIN. We expected that our method can be used for UAV image mosaicking robust to mismatching factors.

ACKNOWLEDGEMENTS

This study was carried out with the support of “Cooperative Research Program for Agriculture Science and Technology Development (Project No. PJ0162332022)” Rural Development Administration, Republic of Korea.

REFERENCES

Li, L., Yao, J., Liu, Y., Yuan, W., Shi, S., and Yuan, S., 2017. Optimal seamline detection for orthoimage mosaicking by combining deep convolutional neural network and graph cuts. *Remote Sensing*, 9(7), 701.

Yoon, S., Kim, T., 2022. TIN-based Robust Mosaicking of UAV images with consecutive image connection. *International Archives of the Photogrammetry, Remote Sensing & Spatial Information Sciences*.

Yuan, Y., Fang, F., and Zhang, G., 2020a. Superpixel-based seamless image stitching for UAV images. *IEEE transactions on geoscience and remote sensing*, 59(2), 1565–1576.

Yuan, S., Yang, K., Li, X., and Cai, H., 2020b. Automatic seamline determination for urban image mosaicking based on road probability map from the D-LinkNet neural network. *Sensors*, 20(7), 1832.

Zhang, W., Guo, B., Li, M., Liao, X., and Li, W., 2018. Improved seam-line searching algorithm for UAV image mosaic with optical flow. *Sensors*, 18(4), 1214.

Zhang, J., Xu, S., Zhao, Y., Sun, J., Xu, S., and Zhang, X., 2023. Aerial orthoimage generation for UAV remote sensing. *Information Fusion*, 89, 91–120.